Original Article

Feasibility analysis of magnetic resonance imaging-based radiomics features for preoperative prediction of nuclear grading of ductal carcinoma in situ

Meng-Ran Zhao[1#], Wen-Juan Ma[2#], Xiang-Chao Song[1], Zhi-Jun Li[1], Zhen-Zhen Shao[2], Hong Lu[2], Rui Zhao[2], Yi-Jun Guo[2], Zhao-Xiang Ye[1*], Pei-Fang Liu[2*]

[1]Department of Radiology, Tianjin Medical University Cancer Institute & Hospital, National Clinical Research Center for Cancer, Tianjin's Clinical Research Center for Cancer, Key Laboratory of Breast Cancer Prevention and Therapy, Tianjin Medical University, Ministry of Education, Key Laboratory of Cancer Prevention and Therapy, Tianjin, China; [2]Department of Breast Imaging, Tianjin Medical University Cancer Institute & Hospital, National Clinical Research Center for Cancer, Tianjin's Clinical Research Center for Cancer, Key Laboratory of Breast Cancer Prevention and Therapy, Tianjin Medical University, Ministry of Education, Key Laboratory of Cancer Prevention and Therapy, Tianjin, China

Contributions: (I) Conception and design: MR Zhao, WJ Ma; (II) Administrative support: H Lu, ZX Ye, PF Liu; (III) Provision of study materials or patients: MR Zhao, XC Song; (IV) Collection and assembly of data: MR Zhao, XC Song, R Zhao; (V) Data analysis and interpretation: MR Zhao, WJ Ma; (VI) Manuscript writing: All authors; (VII) Final approval of manuscript: All authors

[#]These authors contributed equally to this work and should be considered as co-first authors.

[*]These authors contributed equally to this work.

Correspondence to: Pei-Fang Liu, PhD. Department of Breast Imaging, Tianjin Medical University Cancer Institute & Hospital, National Clinical Research Center for Cancer, Tianjin's Clinical Research Center for Cancer, Key Laboratory of Breast Cancer Prevention and Therapy, Tianjin Medical University, Ministry of Education, Key Laboratory of Cancer Prevention and Therapy, Huan-Hu-Xi Road, Ti-Yuan-Bei, Hexi District, Tianjin 300060, China. Email: liupf2017@126.com; Zhao-Xiang Ye, MD. Department of Radiology, Tianjin Medical University Cancer Institute & Hospital, National Clinical Research Center for Cancer, Tianjin's Clinical Research Center for Cancer, Key Laboratory of Breast Cancer Prevention and Therapy, Tianjin Medical University, Ministry of Education, Key Laboratory of Cancer Prevention and Therapy, Huan-Hu-Xi Road, Ti-Yuan-Bei, Hexi District, Tianjin 300060, China. Email: zye@tmu.edu.cn.

Background: The nuclear grading of ductal carcinoma in situ (DCIS) affects its clinical risk. The aim of this study was to investigate the possibility of predicting the nuclear grading of DCIS, by magnetic resonance imaging (MRI)-based radiomics features. And to develop a nomogram combining radiomics features and MRI semantic features to explore the potential role of MRI radiomic features in the assessment of DCIS nuclear grading.

Methods: A total of 156 patients (159 lesions) with DCIS and DCIS with microinvasive (DCIS-MI) were enrolled in this retrospective study, with 112 lesions included in the training cohort and 47 lesions included in the validation cohort. Radiomics features were extracted from Dynamic contrast-enhanced MRI (DCE-MRI) phases 1st and 5th. After feature selection, radiomics signature was constructed and radiomics score (Rad-score) was calculated. Multivariate analysis was used to identify MRI semantic features that were significantly associated with DCIS nuclear grading and combined with Rad-score to construct a Nomogram. Receiver operating characteristic curves were used to evaluate the predictive performance of Rad-score and Nomogram, and decision curve analysis (DCA) was used to evaluate the clinical utility.

Results: In multivariate analyses of MRI semantic features, larger tumor size and heterogeneous enhancement pattern were significantly associated with high-nuclear grade DCIS (HNG DCIS). In the training cohort, Nomogram had an area under curve (AUC) of 0.879 and Rad-score had an AUC of 0.828. Similarly, in the independent validation cohort, Nomogram had an AUC value of 0.828 and Rad-score had an AUC of 0.772. In both the training and validation cohorts, Nomogram had a significantly higher AUC value than Rad-score (P<0.05). DCA confirmed that Nomogram had a higher net clinical benefit.

Conclusions: MRI-based radiomic features can be used as potential biomarkers for assessing nuclear grading of DCIS. The nomogram constructed by radiomic features combined with semantic features is

feasible in discriminating non-HNG and HNG DCIS.

Keywords: Breast cancer; magnetic resonance imaging (MRI); ductal carcinoma in situ (DCIS); radiomics; machine learning

Submitted Mar 29, 2023. Accepted for publication Aug 27, 2023. Published online Sep 19, 2023.
doi: 10.21037/gs-23-132
View this article at: https://dx.doi.org/10.21037/gs-23-132

Introduction

With the routine use of screening mammography, the incidence of ductal carcinoma in situ (DCIS) has increased significantly in recent years (1,2). The overall prognosis of DCIS is excellent, and it is generally accepted clinically that DCIS is largely curable by wide local excision (WLE) (3,4). However, due to its high heterogeneity, non-high nuclear grade DCIS (non-HNG DCIS) often do not progress or progress very slowly and may not be life-threatening, leading to concerns about overtreatment by patients and surgeons (5). In contrast, high-nuclear grade DCIS (HNG DCIS) and DCIS with microinvasive (DCIS-MI), an invasive carcinoma transitional disease with significant correlation to HNG DCIS, have a high incidence of progression to invasive carcinoma and local invasive recurrence, requiring early surgical resection to avoid further disease progression (6-8). Therefore, we need to explore a reliable method for early differentiation of potentially life-threatening HNG DCIS from apparently slow-progressing non-HNG DCIS to provide further pre-treatment supporting information. Therefore, we need an accurate predictive tool to classify potentially life-threatening HNG DCIS and apparently slowly progressing non-HNG DCIS.

Dynamic contrast-enhanced magnetic resonance imaging (DCE-MRI) allows for early diagnosis of breast cancer lesions by injecting contrast agents to rapidly enhance the lesion locally, thus showing the morphological and hemodynamic characteristics of the breast cancer. Compared to mammography and ultrasound, MRI can indeed diagnose DCIS prospectively and can even detect DCIS that cannot be detected by mammography (9). As a result, the clinical trend is increasingly towards the use of MRI for the early diagnosis, preoperative assessment and clinical staging of DCIS (10). Radiomics is the extraction of large amounts of quantitative data from medical radiographic images for use as an aid in the diagnosis, classification or grading of disease (11-13). In previous studies, quantitative radiomics features have obtained relatively favorable performance in predicting the DCIS component in invasive carcinoma and in predicting DCIS recurrence in the ipsilateral breast (14,15). However, relatively few studies have been conducted on the predictive ability of DCE-MRI radiomics features for nuclear grading of DCIS.

Therefore, the purpose of this study was to investigate the possibility of predicting the nuclear grading of DCIS by MRI-based radiomics features. And to develop a nomogram combining radiomics features and MRI semantic features to explore the potential role of MRI radiomic features in the assessment of DCIS nuclear grading. We present this article in accordance with the TRIPOD reporting checklist (available at https://gs.amegroups.com/article/view/10.21037/gs-23-132/rc).

Highlight box

Key findings

- The results of this study show that magnetic resonance imaging (MRI)-based radiomics features can effectively distinguish non-high nuclear grade ductal carcinoma in situ (non-HNG DCIS) from HNG DCIS.

What is known and what is new?

- We already knew that MRI has advantages in the early diagnosis and clinical staging of DCIS.
- In our study, a combination of MRI semantic features and radiomics features was used to construct a Nomogram for predicting the nuclear classification of DCIS.

What is the implication, and what should change now?

- Our data suggest that quantitative MRI-based radiomic features can be used as potential biomarkers reflecting tumor heterogeneity and have clinical value and feasibility in evaluating nuclear grading of DCIS. Moreover, the nomogram constructed by radiomic features combined with semantic features has higher discriminatory ability in identifying non-HNG and HNG DCIS. It is suggested that the nomogram may be useful in future work for optimizing clinical decision making in DCIS patients.

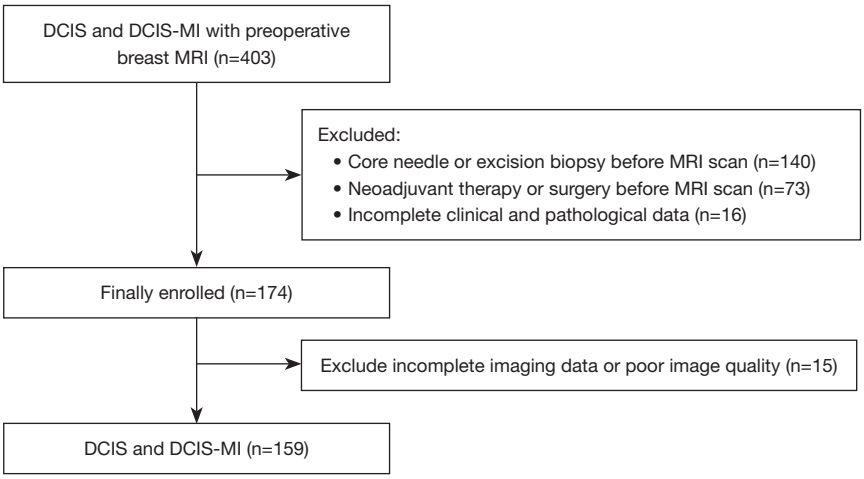

Figure 1 Flow chart of the lesion selection. n, lesion number. DCIS, ductal carcinoma in situ; DCIS-MI, ductal carcinoma in situ with microinvasive; MRI, magnetic resonance imaging.

Methods

Patients

We retrospectively analyzed all DCIS and DCIS-MI patients confirmed by pathology from January 2015 to April 2020 at Tianjin Medical University Cancer Institute & Hospital retrospectively. Inclusion criteria: (I) cases with DCIS and DCIS-MI confirmed by surgical pathology; (II) complete pathology data; (III) obtained a pre-operative breast MRI at our institution. Exclusion criteria: (I) patients who underwent a core needle biopsy or excision biopsy prior to an MRI scan; (II) patients who underwent neoadjuvant therapy prior to surgery; (III) patients with incomplete imaging data or poor image quality (*Figure 1*). In the research, DCIS of low grade and intermediate grade was defined as non-HNG DCIS group. DCIS of high grade or DCIS-MI was defined as HNG DCIS group. This study was conducted in accordance with the Declaration of Helsinki (as revised in 2013). The institutional ethics committee board of Tianjin Medical University Cancer Institute & Hospital (No. Ek2018125) approved this retrospective study and waived the requirement for informed consent.

MRI protocol

MRIs were performed using 1.5T (GE Signa HDxt) or 3.0 T MRI system (GE Discovery MR750, GE Medical Systems, USA). The eight-channel phase-array breast coil was used, and patients were in prone position. The standard protocol consisted of: (I) axial T1-weighted fast-spin-echo sequence (FSE-T_1WI) [repetition time (TR) =622 ms, echo time (TE) =10 ms, matrix size 320×224, section thickness 4.5 mm, field of view (FOV) =29 cm × 29 cm] and T2-weighted fat-suppressed sequence (FS-T_2WI) (TR =6,330 ms, TE =68 ms, matrix size 320×224, section thickness 4.5 mm, FOV =29 cm × 29 cm), (II) diffusion-weighted images (DWI) (TR =3,120 ms, TE =64 ms; matrix size 128×128; slice thickness 4.5 mm, FOV =29 cm × 29 cm) were obtained at b-values of 0, 500, and 1,000 s/mm^2, (III) sagittal dynamic contrast enhancement MRI (DCE-MRI) was obtained by the volume imaging for breast assessment bilateral breast imaging technique (TR =6.1 ms, TE =2.9 ms; matrix size 256×128; slice thickness 1.8 mm, FOV =26 cm × 26 cm). After injecting a contrast agent (Gd-DTPA, 0.2 mL/kg, injection rate 2 mL/s), five-phase contrast-enhanced images were acquired, with each phase lasting approximately 90 s.

MRI analysis

The Functool software on GE AW 4.6 workstation was utilized to evaluate MRI semantic features. Two experienced radiologists (with 3 and 12 years of breast MRI diagnostic experience) analyzed all MR images independently, blinded to the radiological and histopathological information. In case of disagreement, a senior breast imaging doctor would be consulted to reach an agreement. MRI semantic features were evaluated according to the 2013 Breast Imaging Reporting and Data System (BI-RADS) atlas (16)

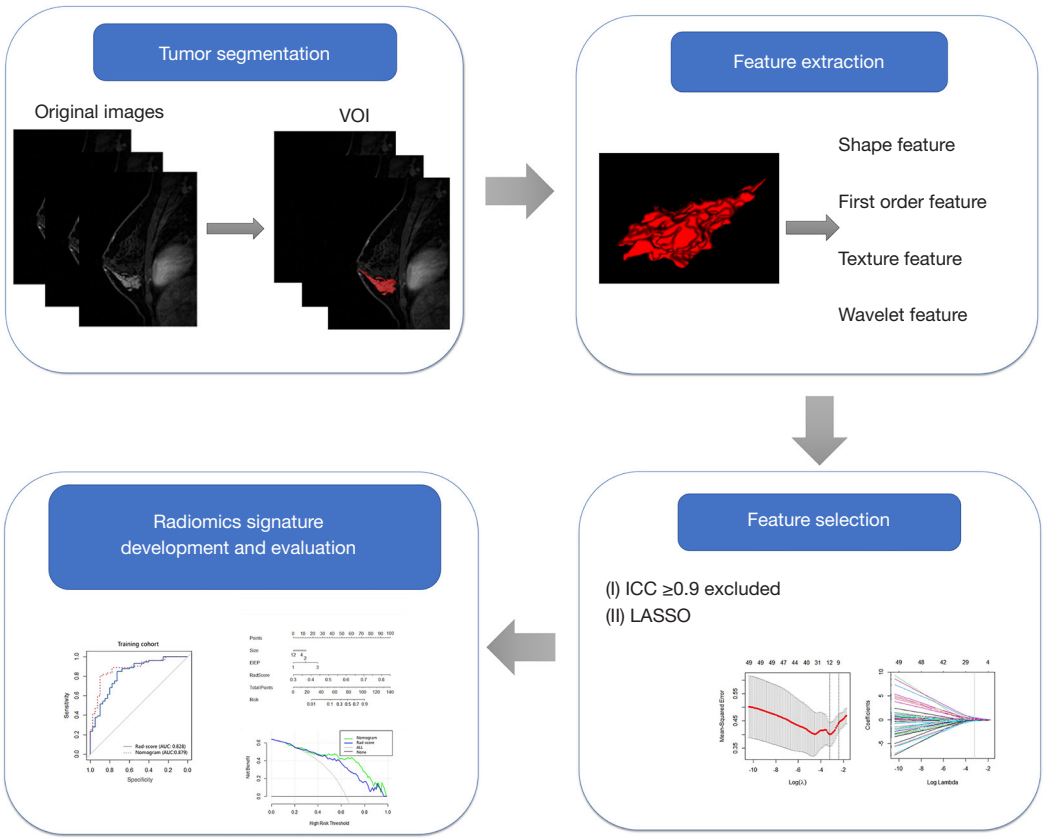

Figure 2 Flow chart of radiomics signature construction. VOI, volume of interest; ICC, intraclass correlation coefficient; LASSO, least absolute shrinkage and selection operator.

proposed by the American College of Radiology (ACR), including tumor size, morphologic features (enhancement distribution, internal enhancement pattern) along with kinetic patterns. DWI signal and apparent diffusion coefficient (ADC) values were also analyzed in this study. The ADC value in the ROI is automatically measured in the workstation. For measuring the lesion size, the largest section of the tumor was selected by reconstructing the three-dimensional (3D) volume of the tumor by three-dimensional maximum intensity projection (3D-MIP) reconstruction of the DCE-MRI images of 1st- and delayed-phase and the largest diameter was used for subsequent analyses.

Development of the radiomics signature

The main flow chart for the development of the radiomics signature is shown in *Figure 2*.

Tumor segmentation

Manual slice-by-slice segmentation of the tumor was performed by a radiologist (Reader 1) using ITK-snap software (https://www.itksnap.org/) in DCE-MRI phases 1st and 5th to obtain the volume of interest (VOI) of the tumor. To further demonstrate the reproducibility of the segmentation, 20 lesions were randomly selected using non-HNG and HNG DCIS as stratification factors to form the reproducibility evaluation dataset. One month later, the tumors were re-segmented by that radiologist (Reader 1) and another radiologist (Reader 2) for validation of intra- and inter-group correlation, respectively. Extraction of radiomics features was performed after image resampling (1×1×1 mm^3 voxel space size) and grey-scale normalization.

Radiomics feature extraction and selection

Python (version 3.5) was used to extract radiomics features,

and R (version 3.6.4) was used for statistical analysis and prediction model construction. In this study, the following three steps were followed to extract robust radiomics features and construct radiomics signatures.

(I) Firstly, the Wilcox rank sum test was used to select radiomics features that were highly related to the nuclear grading of DCIS. The threshold was set at the 0.05 level of significance ($P<0.05$). Features with a hypothesis test of $P\geq0.05$ will not be included in subsequent analyses.

(II) Secondly, to reduce redundancy of high-dimensional features, intra- and inter-group correlation between Reader 1 and Reader 2 was analyzed using intraclass correlation coefficient (ICC), and radiomics features with ICC values ≤0.9 were excluded.

(III) Finally, the most effective prognostic combination of features was chosen using the least absolute shrinkage and selection operator (LASSO) regression approach. The LASSO procedure consists of choosing a regular parameter (λ) and determining the number of features. The tuning regularization parameter λ used to control the strength of the regularization was selected using the one-standard error of the minimum criteria (the 1–SE criteria) chosen for 10-fold cross-validation as a way to mitigate overfitting.

Radiomics signature construction

The radiomics score (Rad-score) for each patient is calculated by a linear combination of the non-zero coefficients of the radiomics features selected by the LASSO regression algorithm as described above, weighted by their respective coefficients.

Radiomics nomogram construction

A radiomics nomogram with Rad-score combined with independent MRI semantic factors was constructed using a multivariate logistic regression algorithm to differentiate between non-HNG and HNG DCIS. Nomogram was established by R (version 3.6.4).

Statistical analysis

Python (version 3.5), R (version 3.6.4) and SPSS software (version 25.0) were used for statistical analysis, with a two-tailed $P<0.05$ being considered statistically significant. Consistency of continuous variables was assessed using ICC analysis of two radiologists and Cohen's Kappa and weighted Kappa analysis of categorical variables. As for the grading of consistency analysis, ICC value less than 0.40 is considered as poor, 0.40–0.54 as weak, 0.55–0.69 as moderate, 0.70–0.84 as good, and greater than 0.85 as excellent; Kappa values below 0.20 are slight, 0.21–0.40 fair, 0.41–0.60 moderate, 0.61–0.80 substantial, and 0.81–1.00 almost perfect (17). Kolmogorov-Smirnov test was used to determine whether the quantitative data obeyed normal distribution. When appropriate, Student's *t*-test, chi-squared test, Fisher's exact test and Mann-Whitney *U* test were used to analyze the differences in MRI semantic features between the non-HNG DCIS and HNG DCIS groups. Significant factors from the univariate analysis were included in the multivariate analysis. Binary Logistics regression analysis was used to identify independent factors associated with the HNG DCIS. ROC curves were plotted to evaluate the predictive performance of Rad-score and Nomogram, and area under curve (AUC), sensitivity, specificity and accuracy were calculated. The integrated discrimination improvement (IDI) was used to compare the differences in AUC between models for statistical significance. Decision curve analysis (DCA) were used to assess the clinical utility of Rad-score and Nomogram.

Results

Patient characteristics

A total of 159 lesions from 156 patients were included in this study, including two patients with bilateral breast cancer and one with a multicentric lesion in the ipsilateral breast. After random selection, 112 (70%) lesions were classified as training cohort, including 40 (35.7%) non-HNG DCIS and 72 (64.3%) HNG DCIS, and 47 (30%) lesions were classified as validation cohort, including 16 (34.0%) non-HNG DCIS and 31 (66.0%) HNG DCIS.

Selection of MRI semantic features

In the training cohort, the tumor size in the HNG DCIS group was significantly larger than the non-HNG DCIS group ($P<0.001$). HNG DCIS generally had lower signal on non-enhanced T1-weighted images ($P=0.015$). In terms of DCE-MRI enhancement distribution, the HNG DCIS group showed more segmental (54.2%, 39/72), while the non-HNG DCIS group showed more focal (40.0%, 16/40) ($P=0.008$). At the early stage of enhancement, the internal

enhancement pattern within the HNG DCIS group was more heterogeneous (77.8%, 56/72), while the non-HNG DCIS group was more clumped (40.0%, 16/40) (P<0.001). As for the time signal intensity curve (TIC) type, plateauing and washout (84.7%, 61/72) were seen more often in the HNG DCIS group and persistent more often in non-HNG DCIS group (P=0.033). The differences in fat-saturated T2-weighted image signal, clustered ring enhancement pattern in delay enhancement phase, DWI signal, and ADC values between the two groups were not statistically significant (P>0.05).

In the validation cohort, the differences in tumor size, enhancement distribution, internal enhancement pattern, and TIC type were statistically significant between the two groups (P<0.05). The detailed description of the clinical and radiological characteristics is provided in *Table 1*. Examples of HNG DCIS and non-HNG DCIS in MRI are shown in *Figures 3,4*.

Based on multivariant analysis, greater tumor size [odds ratio (OR) =1.483, 95% confidence interval (CI): 1.041–2.113; P=0.029] and heterogeneous enhancement pattern (OR =5.502, 95% CI: 1.638–18.482; P=0.006) were significant predictive factors of HNG-DCIS (*Table 2*).

Selection radiomics feature and construction of radiomics signature

After Wilcox rank sum test and ICC analyses, a total of 1,668 radiomics features with potential discriminatory power were selected into the subsequent analyses, including First Order Statistics (19 features), Shape-based (3D) (16 features), Shape-based (2D) (10 features), Gray Level Cooccurence Matrix (Glcm) (24 features), Gray Level Run Length Matrix (Glrlm) (16 features), Gray Level Size Zone Matrix (Glszm) (16 features), Gray Level Dependence Matrix (Gldm) (14 features) and Neighbouring Gray Tone Difference Matrix (Ngtdm) (5 features). The above high-dimensional radiomics features were then incorporated into the LASSO regression algorithm for compression and dimensionality reduction to avoid overfitting and to improve computational efficiency. The plot of mean squared error versus log(λ) (*Figure 5A*) shows that log(λ) takes a value of –2.386 using the 1–SE criterion, corresponding to an optimal λ value of 0.092, allowing the 12 features with non-zero coefficients in the LASSO coefficient curve (*Figure 5B*) to be selected for inclusion in the final radiomics signature construction. Rad-score was determined by adding the weighted total of the specified features. The final formula of Rad-score is:

$$\begin{aligned} Rad\text{-}score = {} & 0.75857339 \\ & -0.10446418*1\_lbp.3D.k\_glcm\_Imc2 \\ & +0.50657631*1\_lbp.3D.k\_glrlm\_ShortRunEmphasis \\ & -0.11624069*1\_wavelet.LLH\_glszm\_SizeZoneNonUniformityNormalized \\ & -0.18994585*1\_wavelet.LHL\_gldm\_DependenceNonUniformityNormalized \\ & +0.25438594*1\_wavelet.HLH\_glszm\_GrayLevelNonUniformityNormalized \\ & -0.11573928*1\_wavelet.HLH\_glszm\_SizeZoneNonUniformityNormalized \\ & -0.31067224*1\_wavelet.HHH\_firstorder\_Minimum \\ & -0.15990086*5\_original\_shape\_Flatness \\ & +0.29638211*5\_wavelet.LLH\_glrlm\_ShortRunLowGrayLevelEmphasis \\ & +0.12334223*5\_wavelet.LLH\_glszm\_ZoneVariance \\ & +0.09791526*5\_wavelet.LHL\_glszm\_SmallAreaLowGrayLevelEmphasis \\ & +0.41061879*5\_wavelet.HHH\_firstorder\_Skewness \end{aligned} \quad [1]$$

Evaluation of predictive performance

After combining Rad-score, tumor size and early internal enhancement pattern features, a Nomogram for predicting DCIS nuclear grading was constructed (*Figure 6*). The scores for each variable were summed to calculate the final nomogram score. The higher the score, the higher the risk of HNG DCIS. The ROC analysis of the predictive efficacy of Rad-score and Nomogram for DCIS nuclear grading is shown in *Figure 7A,7B*. The results show that in the training cohort, the AUC value of the Nomogram (0.879, 95% CI: 0.812–0.946) was significantly higher than the AUC value of the Rad-score (0.828, 95% CI: 0.748–0.909) (P<0.001). Similarly, in the independent validation cohort, the AUC value of the Nomogram (0.819, 95% CI: 0.684–0.953) was significantly higher than the AUC value of the Rad-score (0.772, 95% CI: 0.620–0.924) (P=0.013). In the training cohort, the sensitivity, specificity, and accuracy of the Nomogram and Rad-score for identifying HNG DCIS were 0.720, 0.936, 0.839, and 0.725, 0.847, and 0.804, respectively. In the validation cohort, the sensitivity, specificity and accuracy of the Nomogram and Rad-score for identifying HNG DCIS were 0.733, 0.844, 0.809 and 0.600, 0.852, 0.745, respectively. The diagnostic efficacy of Rad-score and Nomogram in predicting DCIS nuclear grading is summarized in *Table 3*. The DCA (*Figure 7*) results for both models showed that for the differentiation between non-HNG DCIS and HNG DCIS, the Nomogram had a higher overall net benefit than the Rad-score over most of the range of reasonable threshold probabilities. On this basis, we believe that the Nomogram developed in this study can be used as a reliable clinical diagnostic tool for discriminating non-HNG DCIS from HNG DCIS.

Table 1 Univariate analyses for MRI semantic features of HNG DCIS and non-HNG DCIS patients

MRI semantic features	Training cohort			Validation cohort		
	Pathological nuclear grading		P value	Pathological nuclear grading		P value
	Non-HNG DCIS (n=40)	HNG DCIS (n=72)		Non-HNG DCIS (n=16)	HNG DCIS (n=31)	
Tumor size (cm)	2.5 (1.4, 3.5)	4.7 (2.8, 6.4)	<0.001*	1.8 (1.3, 3.0)	4.1 (2.9, 6.2)	0.001*
Age (years)	49.7±10.6	46.8±9.0	0.121	47.1±7.9	45.3±8.0	0.473
T_1WI signals			0.015*			0.168
Slightly lower	9 (22.5)	33 (54.2)		2 (12.5)	11 (35.5)	
Not obvious	31 (77.5)	39 (45.8)		14 (87.5)	20 (64.5)	
T_2WI signals			0.631			
Slightly higher	23 (57.5)	38(52.8)		3 (18.8)	14 (45.2)	0.111
Not obvious	17 (42.5)	34 (47.2)		13 (81.2)	17 (54.8)	
Enhancement distribution			0.015*			0.018*
Focal	20 (50.0)	9 (23.6)		8 (50.0)	5 (16.1)	
Linear	7 (17.5)	10 (13.9)		4 (25.0)	6 (19.4)	
Segmental	12 (30.0)	39 (54.2)		2 (12.5)	17 (54.8)	
Regional	1 (2.5)	6 (8.3)		2 (12.5)	3 (9.7)	
Early internal enhancement patterns			<0.001*			0.001*
Clumped	16 (40.0)	9 (12.5)		7 (43.8)	2 (6.5)	
Homogeneous	14 (35.0)	7 (9.7)		3 (18.8)	2 (6.5)	
Heterogeneous	10 (25.0)	56 (77.8)		6 (37.5)	27 (87.1)	
Clustered ring enhancement patterns in delay phase			0.425			0.209
Presence	12 (30.0)	27 (37.5)		4 (25.0)	15 (48.4)	
Absence	28 (70.0)	45 (62.5)		12 (75.0)	16 (51.6)	
TIC type			0.033*			<0.001*
Persistent	13 (32.5)	11 (15.3)		8 (50.0)	1 (3.2)	
Plateau + washout	27 (67.5)	61 (84.7)		8 (50.0)	30 (96.8)	
DWI			1.000			1.000
Slightly higher	40 (100.0)	71 (98.6)		16 (100.0)	30 (96.8)	
Not obvious	0 (0)	1 (1.4)		0 (0)	1 (3.2)	
ADC value (b =500)	1.30±0.23	1.39±0.28	0.077	1.32±0.26	1.37±0.27	0.490
ADC value (b =1,000)	1.18±0.20	1.23±0.24	0.300	1.16±0.25	1.21±0.26	0.473

Data are presented as n (%), mean ± standard deviation or median (interquartile range). *, denote P<0.05. MRI, magnetic resonance imaging; HNG DCIS, high nuclear grade DCIS; DCIS, ductal carcinoma in situ; T_1WI, T1-weighted imaging; T_2WI, T2-weighted imaging; TIC, time signal intensity curve; DWI, diffusion-weighted images; ADC, apparent diffusion coefficient.

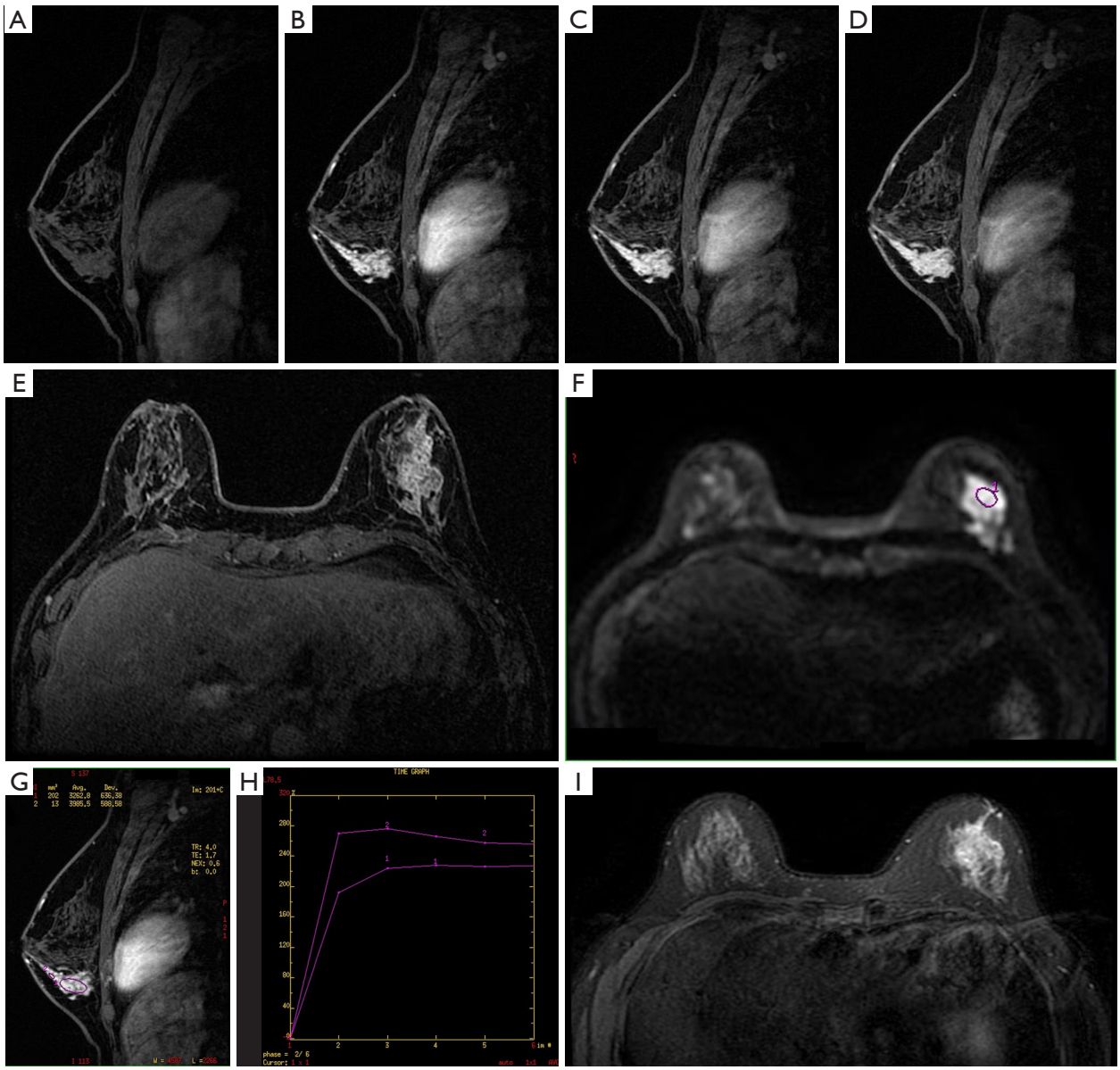

Figure 3 Patient with the left breast HNG DCIS. (A-D) Precontrast and postcontrast sagittal image showed that the lesion was strengthened segmentally, and the internal enhancement pattern was heterogeneous. (E) The axial delayed phase image showed clustered ring enhancement pattern. (F) The lesion showed slightly bright on axial DWI (the purple circle was the region of interest for measuring ADC values). (G-H) The TIC types of the lesion were type II and III (purple circles were regions of interest for measuring TIC). (I) The lesion showed slightly bright on FS-T_2WI. HNG DCIS, high nuclear grade ductal carcinoma in situ; DWI, diffusion-weighted images; ADC, apparent diffusion coefficient; TIC, time signal intensity curve; FS-T_2WI, fat suppression T2-weighted imaging.

Reproducibility of MRI semantic features

In this study, Cohen's Kappa, weighted Kappa and ICC were used to test the consistency between the two radiologists. The consistency of qualitative features between the two radiologists by Cohen's Kappa and weighted Kappa ranged from fair to almost perfect, with the Kappa value from 0.388 (95% CI: 0–0.744) to 0.864 (95% CI: 0.806–0.921), and the consistency of quantitative features calculated by ICC was excellent, with the ICC value ranged from 0.859 (95% CI: 0.744–0.811) to 0.975 (95% CI: 0.965–0.981). Details are provided in *Table 4*.

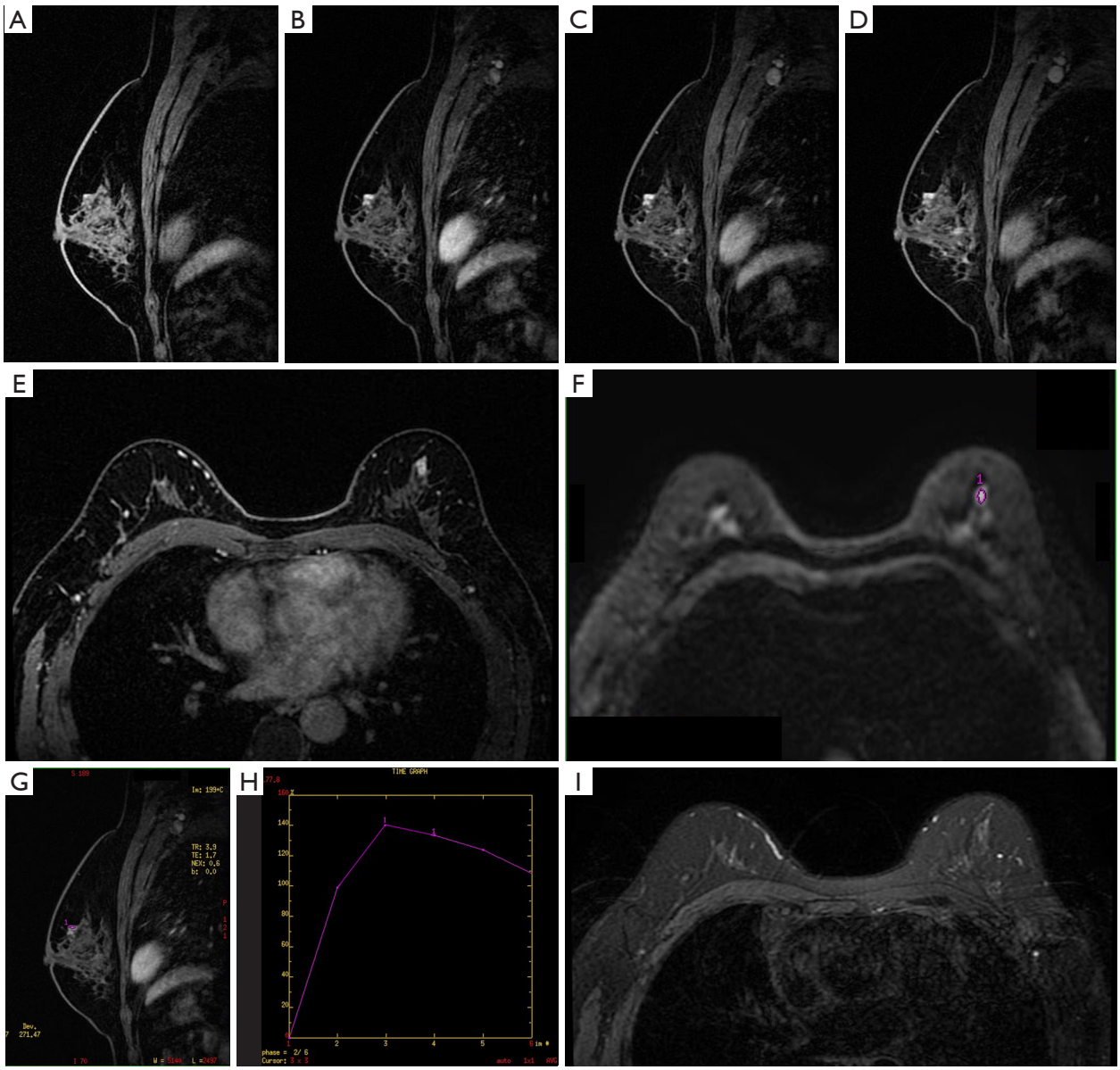

Figure 4 Patient with the left breast non-HNG DCIS. (A-D) Precontrast and postcontrast sagittal image showed that the lesion was strengthened focally, and the internal enhancement pattern was clumped. (E) The axial delayed phase images showed clustered ring enhancement pattern. (F) The lesion showed slightly bright on axial DWI (the purple circle was the region of interest for measuring ADC values). (G,H) TIC types of the lesion were type II and III (the purple circle was region of interest for measuring TIC). (I) The lesion was not obvious on FS-T_2WI. Non-HNG DCIS, non-high nuclear grade ductal carcinoma in situ; DWI, diffusion-weighted images; ADC, apparent diffusion coefficient; TIC, time signal intensity curve; FS-T_2WI, fat suppression T2-weighted imaging.

Discussion

Histological nuclear grading is an important prognostic factor for DCIS, and high nuclear grade is closely associated with its higher local recurrence rate and poor prognosis (18). Early surgical resection is often required for aggressive HNG DCIS to prevent further progression to invasive cancer, whereas for indolent non-HNG DCIS, several large clinical trials are currently exploring the feasibility of conservatively active surveillance for disease management to avoid excessive surgical treatment (5,19,20). Therefore, it

Table 2 Multivariate analysis of predicting DCIS nuclear grading based on MRI semantic features

MRI semantic features	OR	95% CI	P value
Tumor size	1.483	1.041–2.113	0.029*
Early internal enhancement patterns			
Clumped	Reference		
Homogeneous	2.179	0.458–10.372	0.328
Heterogeneous	5.502	1.638–18.482	0.006*
T_1WI signals			
Not obvious	Reference		
Slightly lower	2.196	0.769–6.272	0.142
TIC			
Persistent	Reference		
Plateau + washout	1.835	0.515–6.538	0.349
Enhancement distribution			
Focal	Reference		
Linear	3.538	0.741–16.897	0.113
Segmental	1.042	0.207–5.252	0.961
Regional	1.703	0.103–28.060	0.710

*, denote P<0.05. DCIS, ductal carcinoma in situ; MRI, magnetic resonance imaging; OR, odds ratio; CI, confidence interval; T_1WI, T1-weighted imaging; TIC, time signal intensity curve.

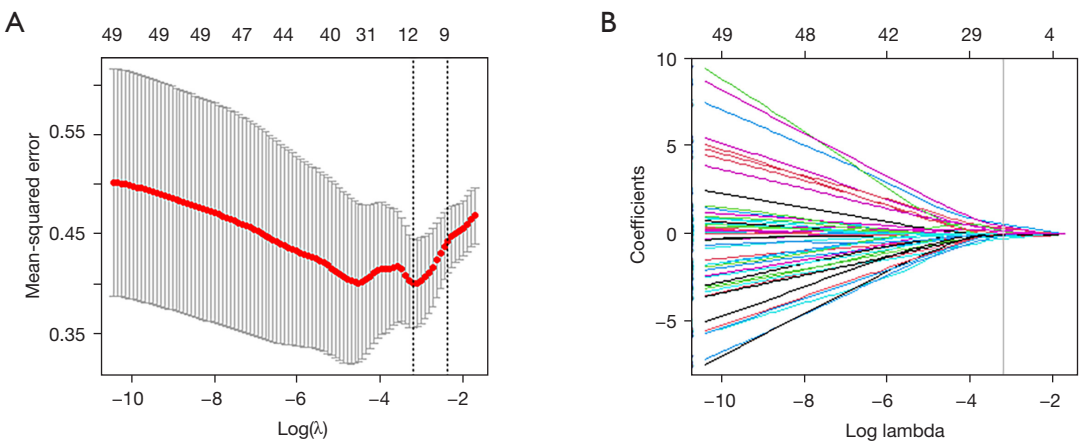

Figure 5 The LASSO regression algorithm selects radiomics features. (A) The tuning parameter (λ) in the LASSO regression algorithm was selected using a 10-fold cross-validated via 1-SE criterion. The optimal log(λ)=−2.386 was determined by plotting the vertical line at the optimal value (right line), corresponding to an optimal λ_1se value of 0.092. (B) Plotting the vertical line at the optimal log(λ) in cross-validation to obtain 12 radiomics features with non-zero coefficients. LASSO, least absolute shrinkage and selection operator; SE, standard error.

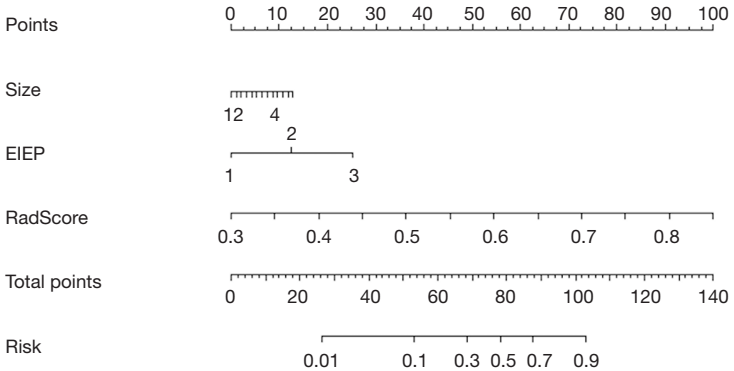

Figure 6 Nomogram predicting the pathological nuclear grading for DCIS. A vertical line is drawn upward from the value of each variable, and the value at the point where it intersects with the scaleplate in the first row is used as the score for that variable. Sum up the scores of each variable to calculate the total nomogram score. Then, using the total score as a starting point, draw a vertical line downward, and the value that intersects with the last line of the scaleplate is the probability of HNG DCIS. The scale of size is mm. EIEP, early internal enhancement patterns; DCIS, ductal carcinoma in situ; HNG, high nuclear grade.

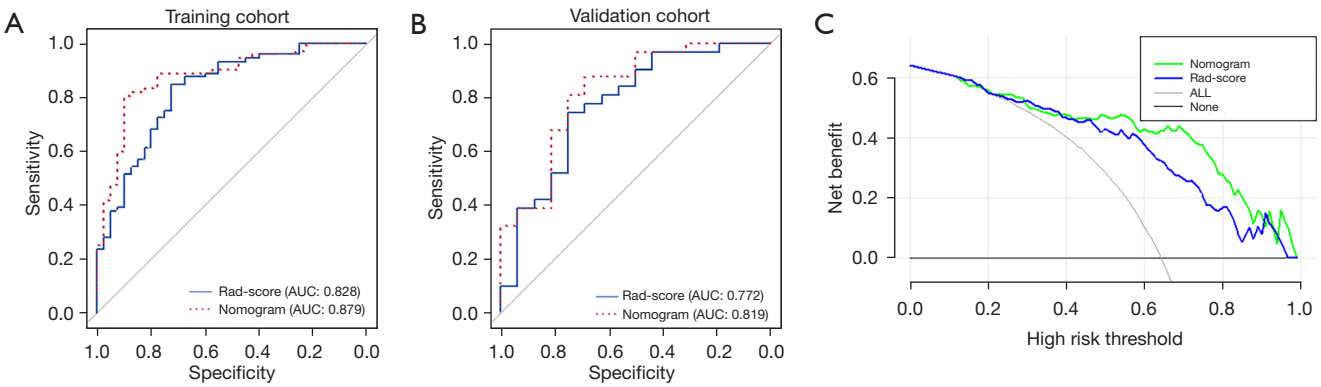

Figure 7 Comparison of ROC curves and DCA between Nomogram and Rad-score for predicting nuclear grading of DCIS. (A) The ROC of training cohort. (B) The ROC of validation cohort. (C) The DCA of Nomogram and Rad-score. AUC, area under curve; ROC, receiver operating characteristic; DCA, decision curve analysis; DCIS, ductal carcinoma in situ.

Table 3 Evaluation of the efficacy of Rad-score and Nomogram in predicting DCIS nuclear grading

Cohort	Rad-score	Nomogram
Training cohort		
AUC	0.828[a] (0.748, 0.909)	0.879[a] (0.812, 0.946)
SEN	0.725 (0.559, 0.849)	0.720 (0.573, 0.833)
SPE	0.847 (0.739, 0.918)	0.936 (0.835, 0.979)
ACC	0.804 (0.718, 0.873)	0.839 (0.758, 0.902)
Validation cohort		
AUC	0.772[b] (0.620, 0.924)	0.819[b] (0.684, 0.953)
SEN	0.600 (0.364, 0.800)	0.733 (0.448, 0.911)
SPE	0.852 (0.654, 0.951)	0.844 (0.665, 0.941)
ACC	0.745 (0.597, 0.861)	0.809 (0.667, 0.909)

Data are presented as N (95% confidence intervals). [a], indicates P<0.001; [b], indicates P=0.013. Rad-score, radiomics score; DCIS, ductal carcinoma in situ; AUC, area under curve; SEN, sensitivity; SPE, specificity; ACC, accuracy.

Table 4 Reproducibility of MRI semantic features

MRI characteristics	Kappa or ICC (95% CI)
Tumor size	0.975 (0.965–0.981)
T_1WI signals	0.715 (0.592–0.819)
T_2WI signals	0.736 (0.623–0.836)
Enhancement modality	0.864 (0.806–0.921)
Early internal enhancement patterns	0.624 (0.503–0.747)
Clustered ring enhancement patterns in delay phase	0.739 (0.613–0.842)
TIC type	0.611 (0.495–0.727)
DWI	0.388 (0–0.744)
ADC value (b =500)	0.865 (0.819–0.899)
ADC value (b =1,000)	0.859 (0.744–0.811)

MRI, magnetic resonance imaging; ICC, intraclass correlation coefficient; CI, confidence interval; T_1WI, T1-weighted imaging; T_2WI, T2-weighted imaging; TIC, time signal intensity curve; DWI, diffusion-weighted images; ADC, apparent diffusion coefficient.

is important to identify MRI characteristics associated with nuclear grading of DCIS and to accurately predict nuclear grading of DCIS in a non-invasive manner. Currently, several clinical trials and studies have explored the unique contribution of MRI in the risk stratification and clinical management of DCIS (21-23). In this study, we found that tumor size, T1-weighted images signal, enhancement distribution, early internal enhancement pattern, and TIC type were significantly correlated with DCIS nuclear grading. In a multivariate analysis, larger tumor size and heterogeneous enhancement pattern were significant predictors for HNG DCIS. In addition, we developed and validated an MRI-based radiomics classifier that can effectively predict DCIS nuclear grading. In particular, the Nomogram combining MRI semantic features and Rad-score provides better ability to discriminate between non-HNG DCIS and HNG DCIS than the single Rad-score.

It is essential to identify the radiological features associated with nuclear grading of DCIS pathology. Compared to conventional mammography and ultrasound, MRI has a higher detection rate for DCIS, with a sensitivity of between 73% and 100% (24,25). In terms of assessing tumor size, MRI is highly correlated with pathology and has a higher measurement accuracy than conventional mammography (26,27). Therefore, it is necessary to further explore in depth potential MRI biomarkers associated with clinical risk of DCIS to differentiate between aggressive and inert DCIS preoperatively. There is evidence in previous studies that DCE-MRI qualitative features can predict DCIS nuclear grading, but there is no consensus (3,28-30).

The larger the malignancy, generally the more aggressive it is (31,32). In previous findings, it was demonstrated that HNG DCIS typically exhibited a greater tumor extent than non-HNG DCIS in MRI (27). Rahbar *et al.* (32) constructed a predictive model for differentiating non-HNG DCIS from HNG DCIS and confirmed that tumor size was a significant factor in differentiating the two in a multivariate analysis (P=0.007). Similar results were shown in our study.

In previous studies, the differences in enhancement patterns within DCE-MRI for DCIS at different nuclear grades have not attracted much attention. However, in this study, we found that the heterogeneity enhancement pattern was a significant predictor of HNG DCIS, and results similar to our study have only been documented in a small number of literatures (33,34). Previous findings suggest that non-mass lesions exhibiting heterogeneous enhancement patterns tend to be more aggressive compared to other enhancement patterns (35). This may be due to the higher density of tumor vessels in more aggressive lesions, which are either rapidly enhanced in the early stages followed by rapid washout, or ischemic necrotic areas that form because of tumor cell aggregation and thus appear as hypointense area (35). When these hypointense areas appear in non-mass enhancement, their internal enhancement pattern automatically shows heterogeneity.

Radiomics is a non-invasive method for quantifying inter- and intra-tumor heterogeneity by extracting high-throughput data from medical images to improve the accuracy of tumor diagnosis and to predict prognosis (11,36). MRI has high soft tissue resolution and multiparametric imaging, and radiomics prediction models based on MRI will have higher diagnostic performance (37,38). DCE-MRI with contrast injection provides a more comprehensive high-dimensional radiomics features and has a higher potential to represent intra-tumor heterogeneity due to the difference in the level of enhancement between the lesion and the background parenchymal enhancement (BPE), allowing for precise segmentation of the lesion margins. In previous studies, radiomics has shown good predictive effects in predicting the infiltrative component in DCIS and in predicting the risk of recurrence of breast cancer (15,39,40). However, at present only a few studies have used MRI-based radiomics features to predict nuclear grading of DCIS. Chou *et al.* suggested HNG DCIS was more

compact and consolidated; as a result, the surface-to-volume ratio of HNG DCIS was smaller than non-HNG DCIS in computer-aided analysis based on MRI (41). In addition, a larger proportion of the 12 radiomics features obtained after feature selection in this study were wavelet-transformed texture features, suggesting that differentiation of high-frequency and low-frequency components of radiomics features extracted from DCE-MRI by image changes can help in the discrimination between non-HNG DCIS and HNG DCIS. In the present study, the Nomogram combining Rad-score and MRI semantic features had high classification ability in predicting DCIS nuclear grading (AUC =0.879 in the training cohort and AUC =0.819 in the validation cohort), and Nomogram had higher prediction performance than single Rad-score ($P<0.05$). The Nomogram combines quantitative radiomics features with MRI semantic features assessed by manual vision to create a classification strategy with high predictive power and also demonstrates the potential of MRI biomarkers to identify clinically and pathologically relevant biological indicators of DCIS.

In addition, the construction of radiomics signature has a high variability in the extraction and selection of quantitative features. A large number of quantitative features extracted from medical images are high-dimensional data, and incorporating all of them into the construction of radiomics signatures often leads to overfitting, thus reducing the accuracy of the classifier (42). In this study, the Wilcox rank sum test, ICC and LASSO regression algorithms were used to reduce the dimensionality of the features for selection and to avoid the impact of redundant features on the robustness of the Rad-score as far as possible.

Aside from the significant results, our current study has some limitations. Firstly, because of the lack of pure DCIS cases, we included DCIS-MI, which was not appropriate to be analyzed together with pure DCIS. Secondly, this is a retrospective study conducted at a single institution. It would be essential to assess whether the current results could be used for imaging data from other medical institutions or further evaluation in larger datasets. Finally, we only extracted the quantitative radiomics features of the first and fifth phase images of DCE-MRI, and did not extract from pre-contrast images and DWI for DCIS classification, which may provide superior information to improve the diagnostic performance.

Conclusions

In summary, we demonstrated that MRI-based radiomic features can be used as a potential biomarker reflecting tumor heterogeneity and have certain clinical value and feasibility in assessing the nuclear grading of DCIS. The nomogram constructed by radiomic features combined with semantic features has the ability to discriminate between non-HNG and HNG DCIS. The nomogram may have potential in future work to assist in optimizing clinical decision making in DCIS patients, but further validation is needed in subsequent work.

Acknowledgments

Funding: This work was supported by the National Key R&D Program of China (Nos. 2017YFC0112600, 2017YFC0112601); Tianjin Science and Technology Major Project (No. 19ZXDBSY00080); National Natural Scientific Foundation of China (No. 81801781); and Tianjin Key Medical Discipline (Specialty) Construction Project (No. TJYXZDXK-009A).

Footnote

Reporting Checklist: The authors have completed the TRIPOD reporting checklist. Available at https://gs.amegroups.com/article/view/10.21037/gs-23-132/rc

Data Sharing Statement: Available at https://gs.amegroups.com/article/view/10.21037/gs-23-132/dss

Peer Review File: Available at https://gs.amegroups.com/article/view/10.21037/gs-23-132/prf

Conflicts of Interest: All authors have completed the ICMJE uniform disclosure form (available at https://gs.amegroups.com/article/view/10.21037/gs-23-132/coif). The authors have no conflicts of interest to declare.

Ethical Statement: The authors are accountable for all aspects of the work in ensuring that questions related to the accuracy or integrity of any part of the work are appropriately investigated and resolved. The study was conducted in accordance with the Declaration of Helsinki (as revised in 2013). The study was approved by institutional ethics committee board of Tianjin Medical University Cancer Institute & Hospital (No. Ek2018125) and individual consent for this retrospective analysis was waived.

Open Access Statement: This is an Open Access article

References

1. Watanabe T, Yamaguchi T, Tsunoda H, et al. Ultrasound Image Classification of Ductal Carcinoma In Situ (DCIS) of the Breast: Analysis of 705 DCIS Lesions. Ultrasound Med Biol 2017;43:918-25.
2. Benveniste AP, Ortiz-Perez T, Ebuoma LO, et al. Is breast magnetic resonance imaging (MRI) useful for diagnosis of additional sites of disease in patients recently diagnosed with pure ductal carcinoma in situ (DCIS)? Eur J Radiol 2017;96:74-9.
3. Esserman LJ, Kumar AS, Herrera AF, et al. Magnetic resonance imaging captures the biology of ductal carcinoma in situ. J Clin Oncol 2006;24:4603-10.
4. Morrow M. The certainties and the uncertainties of ductal carcinoma in situ. J Natl Cancer Inst 2004;96:424-5.
5. Elshof LE, Tryfonidis K, Slaets L, et al. Feasibility of a prospective, randomised, open-label, international multicentre, phase III, non-inferiority trial to assess the safety of active surveillance for low risk ductal carcinoma in situ - The LORD study. Eur J Cancer 2015;51:1497-510.
6. Sanders ME, Schuyler PA, Dupont WD, Page DL. The natural history of low-grade ductal carcinoma in situ of the breast in women treated by biopsy only revealed over 30 years of long-term follow-up. Cancer 2005;103:2481-4.
7. Liu BT, Ding JN, Wang JL, et al. Differences in pathologic characteristics between ductal carcinoma in situ (DCIS), DCIS with microinvasion and DCIS with invasive ductal carcinoma. Int J Clin Exp Pathol 2020;13:1066-72.
8. Champion CD, Ren Y, Thomas SM, et al. DCIS with Microinvasion: Is It In Situ or Invasive Disease? Ann Surg Oncol 2019;26:3124-32.
9. Kuhl CK, Schrading S, Bieling HB, et al. MRI for diagnosis of pure ductal carcinoma in situ: a prospective observational study. Lancet 2007;370:485-92.
10. Clauser P. Clinical value of contralateral breast cancers detected by pre-operative MRI in patients diagnosed with DCIS: a population-based cohort study-commentary. Eur Radiol 2023;33:2207-8.
11. Gillies RJ, Kinahan PE, Hricak H. Radiomics: Images Are More than Pictures, They Are Data. Radiology 2016;278:563-77.
12. Lambin P, Rios-Velazquez E, Leijenaar R, et al. Radiomics: extracting more information from medical images using advanced feature analysis. Eur J Cancer 2012;48:441-6.
13. Ma W, Ji Y, Qi L, et al. Breast cancer Ki67 expression prediction by DCE-MRI radiomics features. Clin Radiol 2018;73:909.e1-909.e5.
14. Xu H, Liu J, Chen Z, et al. Intratumoral and peritumoral radiomics based on dynamic contrast-enhanced MRI for preoperative prediction of intraductal component in invasive breast cancer. Eur Radiol 2022;32:4845-56.
15. Park GE, Kim SH, Lee EB, et al. Ipsilateral Recurrence of DCIS in Relation to Radiomics Features on Contrast Enhanced Breast MRI. Tomography 2022;8:596-606.
16. Morris EA, Comstock CE, Lee CH. ACR BI-RADS® Magnetic Resonance Imaging. In: ACR BI-RADS® Atlas, Breast Imaging Reporting and Data System. Reston, VA, American College of Radiology 2013.
17. Ma Y, Liu A, Zhang Y, et al. Comparison of background parenchymal enhancement (BPE) on contrast-enhanced cone-beam breast CT (CE-CBBCT) and breast MRI. Eur Radiol 2022;32:5773-82.
18. Solin LJ. Counterview: Pre-operative breast MRI (magnetic resonance imaging) is not recommended for all patients with newly diagnosed breast cancer. Breast 2010;19:7-9.
19. Hwang ES, Hyslop T, Lynch T, et al. The COMET (Comparison of Operative versus Monitoring and Endocrine Therapy) trial: a phase III randomised controlled clinical trial for low-risk ductal carcinoma in situ (DCIS). BMJ Open 2019;9:e026797.
20. Francis A, Thomas J, Fallowfield L, et al. Addressing overtreatment of screen detected DCIS; the LORIS trial. Eur J Cancer 2015;51:2296-303.
21. Chou SS, Romanoff J, Lehman CD, et al. Preoperative Breast MRI for Newly Diagnosed Ductal Carcinoma in Situ: Imaging Features and Performance in a Multicenter Setting (ECOG-ACRIN E4112 Trial). Radiology 2021;301:66-77.
22. Lamb LR, Lehman CD, Oseni TO, Bahl M. Ductal Carcinoma In Situ (DCIS) at Breast MRI: Predictors of Upgrade to Invasive Carcinoma. Acad Radiol 2020;27:1394-9.
23. Greenwood HI, Wilmes LJ, Kelil T, et al. Role of Breast MRI in the Evaluation and Detection of DCIS: Opportunities and Challenges. J Magn Reson Imaging

2020;52:697-709.
24. Petrillo A, Fusco R, Petrillo M, et al. Added Value of Breast MRI for Preoperative Diagnosis of Ductal Carcinoma In Situ: Diagnostic Performance on 362 Patients. Clin Breast Cancer 2017;17:e127-34.
25. Kuhl CK, Strobel K, Bieling H, et al. Impact of Preoperative Breast MR Imaging and MR-guided Surgery on Diagnosis and Surgical Outcome of Women with Invasive Breast Cancer with and without DCIS Component. Radiology 2017;284:645-55.
26. Baur A, Bahrs SD, Speck S, et al. Breast MRI of pure ductal carcinoma in situ: sensitivity of diagnosis and influence of lesion characteristics. Eur J Radiol 2013;82:1731-7.
27. Shiraishi M, Igarashi T, Terayama T, et al. Breast magnetic resonance imaging for estimation of the tumour extent in patients with pure ductal carcinoma in situ: Comparison between full diagnostic and abbreviated protocols. Eur J Radiol 2020;123:108788.
28. Tozaki M, Fukuda K. High-spatial-resolution MRI of non-masslike breast lesions: interpretation model based on BI-RADS MRI descriptors. AJR Am J Roentgenol 2006;187:330-7.
29. Facius M, Renz DM, Neubauer H, et al. Characteristics of ductal carcinoma in situ in magnetic resonance imaging. Clin Imaging 2007;31:394-400.
30. Neubauer H, Li M, Kuehne-Heid R, et al. High grade and non-high grade ductal carcinoma in situ on dynamic MR mammography: characteristic findings for signal increase and morphological pattern of enhancement. Br J Radiol 2003;76:3-12.
31. Nori J, Meattini I, Giannotti E, et al. Role of preoperative breast MRI in ductal carcinoma in situ for prediction of the presence and assessment of the extent of occult invasive component. Breast J 2014;20:243-8.
32. Rahbar H, Partridge SC, Demartini WB, et al. In vivo assessment of ductal carcinoma in situ grade: a model incorporating dynamic contrast-enhanced and diffusion-weighted breast MR imaging parameters. Radiology 2012;263:374-82.
33. Tajima CC, de Sousa LLC, Venys GL, et al. Magnetic resonance imaging of the breast: role in the evaluation of ductal carcinoma in situ. Radiol Bras 2019;52:43-7.
34. Jansen SA, Newstead GM, Abe H, et al. Pure ductal carcinoma in situ: kinetic and morphologic MR characteristics compared with mammographic appearance and nuclear grade. Radiology 2007;245:684-91.
35. Machida Y, Shimauchi A, Tozaki M, et al. Descriptors of Malignant Non-mass Enhancement of Breast MRI: Their Correlation to the Presence of Invasion. Acad Radiol 2016;23:687-95.
36. Lambin P, Leijenaar RTH, Deist TM, et al. Radiomics: the bridge between medical imaging and personalized medicine. Nat Rev Clin Oncol 2017;14:749-62.
37. Drukker K, Li H, Antropova N, et al. Most-enhancing tumor volume by MRI radiomics predicts recurrence-free survival "early on" in neoadjuvant treatment of breast cancer. Cancer Imaging 2018;18:12.
38. Fan M, Li H, Wang S, et al. Radiomic analysis reveals DCE-MRI features for prediction of molecular subtypes of breast cancer. PLoS One 2017;12:e0171683.
39. Li J, Song Y, Xu S, et al. Predicting underestimation of ductal carcinoma in situ: a comparison between radiomics and conventional approaches. Int J Comput Assist Radiol Surg 2019;14:709-21.
40. Li H, Zhu Y, Burnside ES, et al. MR Imaging Radiomics Signatures for Predicting the Risk of Breast Cancer Recurrence as Given by Research Versions of MammaPrint, Oncotype DX, and PAM50 Gene Assays. Radiology 2016;281:382-91.
41. Chou SS, Gombos EC, Chikarmane SA, et al. Computer-aided heterogeneity analysis in breast MR imaging assessment of ductal carcinoma in situ: Correlating histologic grade and receptor status. J Magn Reson Imaging 2017;46:1748-59.
42. Ma Q, Yi Y, Liu T, et al. MRI-based radiomics signature for identification of invisible basal cisterns changes in tuberculous meningitis: a preliminary multicenter study. Eur Radiol 2022;32:8659-69.

Cite this article as: Zhao MR, Ma WJ, Song XC, Li ZJ, Shao ZZ, Lu H, Zhao R, Guo YJ, Ye ZX, Liu PF. Feasibility analysis of magnetic resonance imaging-based radiomics features for preoperative prediction of nuclear grading of ductal carcinoma in situ. Gland Surg 2023;12(9):1209-1223. doi: 10.21037/gs-23-132